Modern Physics Letters A
Vol. 23, Nos. 17–20 (2008) 1506–1513

World Scientific
www.worldscientific.com

A MOMENT METHOD FOR MEASURING THE HIGHER-ORDER WEAK GRAVITATIONAL LENSING EFFECTS

KEIICHI UMETSU[1,2], YUKI OKURA[3], TOSHIFUMI FUTAMASE[3]

[1]*Institute of Astronomy and Astrophysics, Academia Sinica, Taipei, Taiwan*
[2]*Leung Center for Cosmology and Particle Astrophysics, National Taiwan University, Taiwan*
[3]*Astronomical Institute, Tohoku University, Sendai, Japan*
keiichi@asiaa.sinica.edu.tw

We present a method for measuring higher-order weak lensing distortions of faint background galaxies, namely the weak gravitational flexion, by fully extending the Kaiser, Squires & Broadhurst method to include higher-order lensing image characteristics (HOLICs) introduced by Okura, Umetsu, & Futamase. Our HOLICs formalism allows accurate measurements of flexion from practical observational data in the presence of non-circular, anisotropic point spread function. We have applied our method to ground-based Subaru observations of the massive galaxy cluster A1689 at a redshift of $z = 0.183$. From the high-precision measurements of spin-1 first flexion, we obtain a high-resolution mass map in the central region of A1689. The reconstructed mass map shows a bimodal feature in the central $4' \times 4'$ region of the cluster. The major, pronounced mass peak is associated with the brightest cluster galaxy and central cluster members, while the secondary peak is associated with a local concentration of bright galaxies. In Fourier space we separate the reconstructed mass distribution into cluster and subhalo components, from which we obtain projected subhalo masses associated with the primary and the secondary peaks to be $M_1 = (2.2 \pm 0.4) \times 10^{13} M_\odot/h$, and $M_2 = (1.1 \pm 0.3) \times 10^{13} M_\odot/h$, respectively.

Keywords: Cosmology: observations; gravitational lensing; galaxies: clusters: individual (Abell 1689).

1. Introduction

Weak gravitational lensing is responsible for the weak shape-distortion and magnification of the images of background sources due to the gravitational field of intervening matter.[1,2] To the first order, weak lensing gives rise to a few – 10% levels of elliptical distortions in images of background sources, responsible for the second-order derivatives of the gravitational lensing potential. Thus, the weak lensing signal, measured from tiny but coherent quadrupole distortions in galaxy shapes, can provide a direct measure of the projected mass distribution of cosmic structures. However, practical weak lensing observations subject to the effects of atmospheric seeing, isotropic and anisotropic point spread function (PSF), and residual camera distortion across the field of view, which must be examined from the stellar shape measurements and corrected for in the weak lensing analysis. Practical methods for

PSF corrections and shear measurements/calibrations have been studied and developed by many authors, such as pioneering work of Kaiser, Squires, & Broadhurst (hereafter KSB).[3]

In recent years, there have been theoretical efforts to include the next higher order distortion effects as well as the usual quadrupole distortion effect in the weak lensing analysis.[4,5,6,7,8,9] We have proposed in Ref. 8 to use certain convenient combinations of octopole/higher multipole moments of background images which we call the Higher Order Lensing Image's Characteristics (HOLICs), and have shown that HOLICs serve as a direct measure for the next higher-order weak lensing effect, or the gravitational flexion[5] and that the use of HOLICs in addition to the quadrupole shape distortions can improve the accuracy and resolution of weak lensing mass reconstructions based on simulated observations.

In the present paper we present a method for measuring flexion by the HOLICs moment approach[9] by fully extending the KSB formalism. We then apply our method to actual, ground-based Subaru observations of A1689, and perform a mass reconstruction in the central region of A1689. The paper is organized as follows. We first summarize in Sec. 2 the basis of weak gravitational lensing and the flexion formalism. We will then present our moment method[8,9] for practical flexion measurements. In Sec. 3 we will perform a weak lensing flexion analysis of A1689 by our fully-extended HOLICs approach, and perform a mass reconstruction of A1689 from the HOLICs estimates of flexion. Finally summary and discussions are given in Sec. 4. We refer interested readers to a complete appendix[a] for details of the derivation of flexion-observable relationships in practical observations.

2. Basis of Weak Lensing and Flexion

2.1. *Weak lensing and flexion formalism*

In this section, we summarize general aspects of weak gravitational lensing and flexion formalism, following the complex derivative notation.[6] A general review of quadrupole weak lensing can be found in Ref. 1.

The gravitational deflection of light rays can be described by the lens equation, $\boldsymbol{\beta} = \boldsymbol{\theta} - \boldsymbol{\nabla}\psi(\boldsymbol{\theta})$, where $\psi(\boldsymbol{\theta})$ is the effective lensing potential, which is defined by the two-dimensional Poisson equation as $\nabla^2\psi(\boldsymbol{\theta}) = 2\kappa(\boldsymbol{\theta})$, with the lensing convergence. Here the convergence $\kappa = \int d\Sigma_m \Sigma_{\rm crit}^{-1}$ is the dimensionless surface mass density projected on the sky, normalized with respect to the critical surface mass density of gravitational lensing, $\frac{c^2}{4\pi G}\frac{D_s}{D_d D_{ds}}$, where D_d, D_s, and D_{ds} are the angular diameter distances from the observer to the deflector, from the observer to the source, and from the deflector to the source, respectively. By introducing the complex gradient operator, $\partial = \partial_1 + i\partial_2$ that transforms as a vector, $\partial' = \partial e^{i\phi}$, with ϕ being the angle of rotation, the lensing convergence κ is expressed as $\kappa = \frac{1}{2}\partial\partial^*\psi$, where * denotes the complex conjugate. Similarly, the complex gravitational shear

[a]Full appendix is available at http://www.asiaa.sinica.edu.tw/keiichi/OUF2/appendix.pdf.

of spin-2 is defined as $\gamma \equiv \gamma_1 + i\gamma_2 = \frac{1}{2}\partial\partial\psi$. The third-order derivatives of $\psi(\boldsymbol{\theta})$ can be combined to form a pair of the complex flexion fields as[6]:

$$\mathcal{F} \equiv \mathcal{F}_1 + i\mathcal{F}_2 = \frac{1}{2}\partial\partial\partial^*\psi\,, \tag{1}$$

$$\mathcal{G} \equiv \mathcal{G}_1 + i\mathcal{G}_2 = \frac{1}{2}\partial\partial\partial\psi\,. \tag{2}$$

If the angular size of an image is small compared to the scale over which the lens potential ψ varies, then we can locally expand the lens equation to have $d\beta_i = \mathcal{A}_{ij}d\theta_j + \frac{1}{2}\mathcal{D}_{ijk}d\theta_j d\theta_k$ to the second order, where $\mathcal{A}_{ij}$ is the Jacobian matrix of the lens equation and $\mathcal{D}_{ijk} = \mathcal{A}_{ij,k} = -\psi_{,ijk}$ is the third-order lensing tensor,

$$\mathcal{A}_{ij} = \begin{pmatrix} 1-\kappa-\gamma_1 & -\gamma_2 \\ -\gamma_2 & 1-\kappa+\gamma_1 \end{pmatrix}, \tag{3}$$

$$\mathcal{D}_{ijk} = \mathcal{F}_{ijk} + \mathcal{G}_{ijk}\,. \tag{4}$$

The third-order tensor $\mathcal{D}_{ijk}$ can be expressed with the sum of the two terms, $\mathcal{D}_{ijk} = \mathcal{F}_{ijk} + \mathcal{G}_{ijk}$, with the spin-1 part $\mathcal{F}_{ijk}$ and the spin-3 part $\mathcal{G}_{ijk}$, composed of the real/imaginary part of the flexion fields:

$$\mathcal{F}_{ij1} = -\frac{1}{2}\begin{pmatrix} 3\mathcal{F}_1 & \mathcal{F}_2 \\ \mathcal{F}_2 & \mathcal{F}_1 \end{pmatrix}, \quad \mathcal{F}_{ij2} = -\frac{1}{2}\begin{pmatrix} \mathcal{F}_2 & \mathcal{F}_1 \\ \mathcal{F}_1 & 3\mathcal{F}_2 \end{pmatrix}, \tag{5}$$

$$\mathcal{G}_{ij1} = -\frac{1}{2}\begin{pmatrix} \mathcal{G}_1 & \mathcal{G}_2 \\ \mathcal{G}_2 & -\mathcal{G}_1 \end{pmatrix}, \quad \mathcal{G}_{ij2} = -\frac{1}{2}\begin{pmatrix} \mathcal{G}_2 & -\mathcal{G}_1 \\ -\mathcal{G}_1 & -\mathcal{G}_2 \end{pmatrix}. \tag{6}$$

Note that flexion has a dimension of inverse length (or inverse angle), meaning that the flexion effect depends on the angular size of the source. The shape quantities affected by the first flexion $\mathcal{F}$ alone have spin-1 properties, while those affected by the second flexion $\mathcal{G}$ alone have spin-3 properties. These third-order lensing fields naturally appear in the transformation equations of HOLICs between the lens and source planes.

2.2. *Flexion observable – HOLICs*

The flexion fields, $\mathcal{F}$ and $\mathcal{G}$, can be measured from proper combinations of higher-order shape moments with the corresponding spin properties and the dimension.[8,9] Higher-order moments of images are defined as a straightforward extension of the quadrupole moment. The octopole moment Q_{ijk} and the 16pole moment Q_{ijkl} are defined as follows:

$$Q_{ijk} \equiv \frac{\int d^2\theta\, q_I[I(\boldsymbol{\theta})]\Delta\theta_i\Delta\theta_j\Delta\theta_k}{\int d^2\theta\, q_I[I(\boldsymbol{\theta})]}\,, \tag{7}$$

$$Q_{ijkl} \equiv \frac{\int d^2\theta\, q_I[I(\boldsymbol{\theta})]\Delta\theta_i\Delta\theta_j\Delta\theta_k\Delta\theta_l}{\int d^2\theta\, q_I[I(\boldsymbol{\theta})]}\,. \tag{8}$$

Then, ζ and δ of the spin-1 and spin-3 HOLICs, respectively, are defined by

$$\begin{aligned}\zeta &\equiv \frac{Q_{111}+Q_{122}+i\,(Q_{112}+Q_{222})}{\xi}\,,\\ \delta &\equiv \frac{Q_{111}-3Q_{122}+i\,(3Q_{112}-Q_{222})}{\xi}\,,\end{aligned} \tag{9}$$

where ξ is the spin-0 normalization factor, $\xi = Q_{1111}+2Q_{1122}+Q_{2222}$.

We have derived in Ref. 8 full transformation equations between unlensed and lensed HOLICs under the sub-critical lensing condition, i.e., $\det\mathcal{A} > 0$. Since the HOLICs ζ and δ are non-zero spin quantities with a direction dependence, the expectation value of the intrinsic ζ and δ are assumed to vanish. To the first order in flexion, we have the linear relations between the HOLICs and flexion fields as

$$\begin{aligned}\mathcal{F} &\approx \left\langle \frac{\zeta}{\frac{9}{4}-3\frac{(\mathrm{tr}Q)^2}{\xi}} \right\rangle,\\ \mathcal{G} &\approx \frac{4}{3}\langle\delta\rangle\,,\end{aligned} \tag{10}$$

where $\mathrm{tr}Q = Q_{11}+Q_{22}$ is the trace of the quadrupole moment, Q_{ij}.

2.3. *Flexion and HOLICs in practical applications*

For a practical application of the HOLICs approach, we must take into account various observational effects such as noise in the shape measurement due to read-out and/or sky background and the dilution of the lensing signal due to the isotropic/anisotropic PSF effects. Thus, one cannot simply use Eq. (10) to measure the flexion fields. In Ref. 9 we have taken into account explicitly the weight function in calculations of noisy shape moments and the effect of higher-order PSF anisotropy, as well as isotropic PSF smearing, and derived relevant transformation equations between unlensed (intrinsic) and lensed (observed) HOLICs. As in the case of quadrupole weak lensing, the linearized transformation equations for flexion can be expressed as follows:

$$\zeta_i = \zeta_i^{(s)} + C_{ij}^{\mathcal{F}}\mathcal{F}_j + C_{ij}^{q}\zeta_j^{q}\,, \tag{11}$$

$$\delta_i = \delta_i^{(s)} + D_{ij}^{\mathcal{G}}\mathcal{G}_j + D_{ij}^{q}\delta_j^{q}\,, \tag{12}$$

where quantities with subscript "(s)" represent those of unlensed, intrinsic background sources, Cs and Ds are linear response coefficients for ζ and δ, respectively, which can be calculated from observable weighted shape moments of galaxies and stellar objects (i.e., PSF), and ζ_q and δ_q are the spin-1 and the spin-3 PSF anisotropy kernels, respectively. Since the expectation values of intrinsic HOLICs are assumed to vanish, we have linear relations between the observed HOLICs and flexion as

$$\mathcal{F} \approx \langle \left(C^{\mathcal{F}}\right)^{-1}(\zeta - C^{q}\zeta_q)\rangle\,, \tag{13}$$

$$\mathcal{G} \approx \langle \left(D^{\mathcal{G}}\right)^{-1}(\delta - D^{q}\delta_q)\rangle\,. \tag{14}$$

2.4. *Flexion analysis of subaru A1689 data*

We apply our flexion analysis method based on the HOLICs moment approach to Subaru imaging observations of the cluster A1689. A1689 is a massive cluster of galaxies at a moderately low redshift of $z = 0.183$, having a large Einstein radius of ≈ 45 arcsec for a background source at $z_s \sim 1$.[10] A1689 is one of the best studied lensing clusters.[10,11,12,13,14,15] The observed strong and weak lensing profiles of A1689 are well fitted by the NFW[16] model with a large virial mass, $M_{\rm vir} \sim 1.4 \times 10^{15} h^{-1} M_\odot$, and a high concentration, $c_{\rm vir} \sim 14$.[11,15]

For our flexion analysis of A1689, we used Suprime-Cam i'-imaging data[11,15] covering a field of $\sim 30' \times 25'$ with $0\farcs202\,{\rm pixel}^{-1}$ sampling. The seeing FWHM in the co-added i' image is $0\farcs88$, and the limiting magnitude is $i' = 25.9$ for a 3σ detection within a $2''$ aperture.[11] Since the flexion signal is weaker at larger angular scales (see Ref. 8 for detailed discussions), in the present flexion analysis we discarded outer boundaries from the analysis and only used the central 3000×3000 pixel region, corresponding an angular scale of $\approx 10'$ on a side, or a physical scale of $1.3h^{-1}$ Mpc at the cluster redshift of $z = 0.183$. We used our weak lensing analysis pipeline based on IMCAT[3] extended to include our HOLICs moment method (see Ref. 9 for details of the weak lensing flexion analysis of A1689). We use our first flexion measurements obtained with our moment-based analysis method to reconstruct the projected mass distribution of A1689. To do this we utilize the Fourier-space relation between the first flexion $\mathcal{F}$ and the lensing convergence κ with the weak lensing approximation.[6,8] The field size for the mass reconstruction is $9' \times 9'$, sampled with a grid of 256×256 pixels, over which the unconstrained $k = 0$ mode is set to zero. Fig. 1 shows the central $4' \times 4'$ region of the dimensionless projected mass distribution (the $\kappa(\boldsymbol{\theta})$ field) of A1689 reconstructed from the observed spin-1 flexion ($\mathcal{F}$) field. The reconstructed κ map was smoothed with a Gaussian filter of FWHM $= 0\farcm33$. The rms error in the mass reconstruction is estimated to be $\sigma \approx 0.51$ from the dispersion in the reconstructed B-mode κ field, which is expected to vanish in the weak lensing limit. Fig. 1 reveals two significant mass concentrations associated with clumps of bright galaxies. The first mass peak has a peak value of $\kappa = 2.66$, and is detected at 5.2σ significance. This first peak is associated with the central concentration of bright cluster galaxies including the cD galaxy, as shown in Fig. 1. This central mass concentration associated with the brightest cluster galaxies was not detected in the earlier ACS flexion analysis.[17] The second peak (4.4σ significance), on the other hand, is located $\approx 0\farcm9$ to the northeast direction, and is associated with a local clump of bright galaxies (see Fig. 1), having a peak value of $\kappa = 2.23$. This second mass peak has been detected in the earlier lensing studies based on the high resolution HST/ACS data.[10,17]

In order to estimate the masses of the subhalos excluding the contribution of the large-scale cluster halo, we separate in Fourier space the reconstructed $\kappa(\boldsymbol{\theta})$ field into cluster and subhalo components. Fig. 2 compares the central mass distributions of the cluster component (left panel) with an angular multipole range of $l \lesssim 12000$

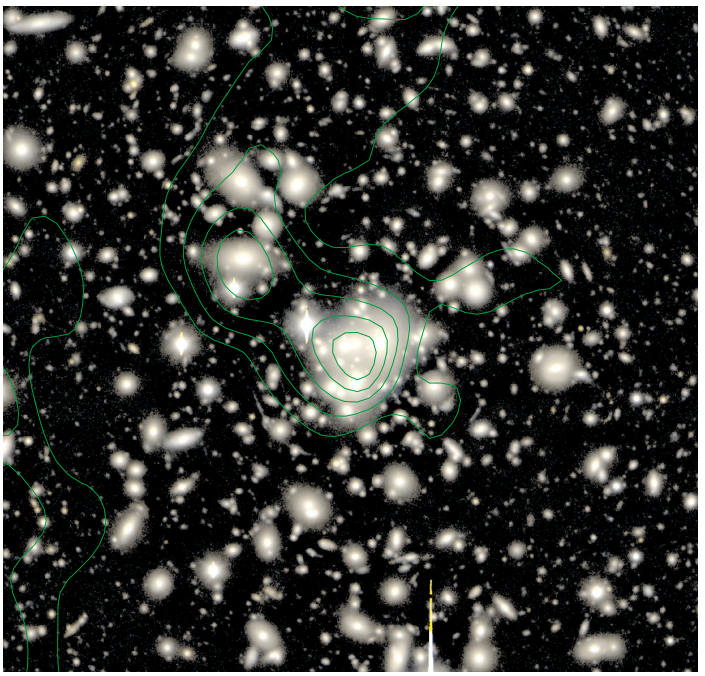

Fig. 1. False-color image of the central $4' \times 4'$ cluster region of A1689 ($z = 0.183$) composed of the Subaru/Suprime-Cam V and i' images. Overlayed are contours of the lensing κ-field reconstructed from the first flexion measurements using the i'-band data. The contours are spaced in units of $1\sigma(\approx 0.51)$ reconstruction error estimated from the rms of the B-mode reconstruction. North is to the top, and East to the left.

and the subhalo component (right panel) with $12000 \lesssim l \lesssim 40000$, where the l-limits are identified based on the power spectrum of the reconstructed κ map. For the concordance cosmology with $\Omega_m = 0.3$ and $\Omega_\Lambda = 0.7$ and a mean background redshift of $z_s = 0.9$, we estimate the projected mass of the central subhalo to be $M_1(< 0'.45) = (2.2 \pm 0.4) \times 10^{13} M_\odot/h$, and the projected mass of the northeast subhalo to be $M_2(< 0'.4) = (1.1 \pm 0.3) \times 10^{13} M_\odot/h$.

3. Discussion and Conclusions

In the paper we have presented a method for weak lensing flexion analysis by fully extending the KSB method to include the measurement of HOLICs.[8,9] In particular, we take into account explicitly the weight function in calculations of noisy shape moments and the effects of spin-1 and spin-3 PSF anisotropies, as well as isotropic PSF smearing, in the limit of weak lensing and small PSF anisotropy (q). We extended the KSB formalism[3] to include the higher-order isotropic and anisotropic PSF effects relevant to spin-1 and spin-3 HOLICs, which provides direct relations between the observable HOLICs and underlying flexion in the weak lensing limit.

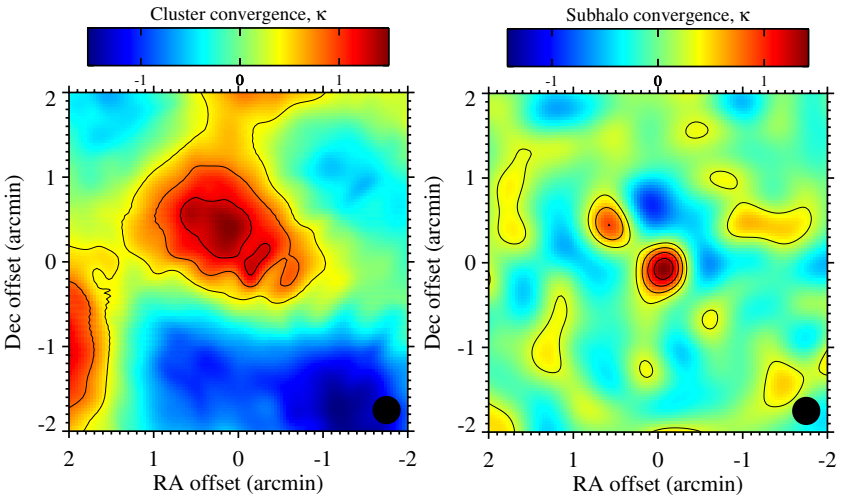

Fig. 2. (*Left*): cluster-halo component with an angular multipole range of $l \lesssim 12000$ in the reconstructed κ field of A1689. (*Right*): small scale subhalo component with $12000 \lesssim l \lesssim 40000$ in the reconstructed κ field. The projected mass of the central subhalo associated with the cD galaxy is estimated as $M_1 = (2.2 \pm 0.4) \times 10^{13} M_\odot/h$, and the projected mass of the northeast subhalo is obtained as $M_2 = (1.1 \pm 0.3) \times 10^{13} M_\odot/h$. The contour levels are in units of 1σ error. The black, solid circle in the lower-right corner indicates the Gaussian FWHM ($= 0.'33$) used for the mass reconstruction. At the cluster redshift of $z = 0.183$, one arcminute corresponds to about 129kpc$/h$.

We have implemented in our analysis pipeline our flexion analysis algorithm based on the HOLICs moment approach, and applied our flexion analysis pipeline to ground-based i' imaging data of the rich cluster A1689 ($z = 0.183$) taken with Subaru/Suprime-Cam. Our mass reconstruction from the first-flexion measurements shows two significant ($> 4\sigma$) mass structures associated with concentrations of bright galaxies in the central cluster region: the first peak (5.2σ) associated with the central concentration of bright galaxies including the cD galaxy, and the second peak (4.4σ) associated with a clump of bright galaxies located $\sim 1'$ northeast of the cluster center. This significant detection of the second peak confirms earlier ACS lensing studies.[10,17] The central mass peak, however, was not recovered in the earlier flexion analysis based on HST/ACS data.[17] In Ref. 17 the authors attributed this failure to their relatively large reconstruction error at the cluster center, although they have a very large number density of background galaxies, $\bar{n}_g \approx 75$ arcmin^{-2}. On the other hand, owing to our conservative selection criteria for the background sample, the mean number density of background galaxies used for the present analysis is $\bar{n}_g = 7.75$ arcmin^{-2}, which is almost one order of magnitude smaller than that of the ACS data, and is about $20\% - 30\%$ of a typical number density of magnitude/size-selected background galaxies usable for the quadrupole shape measurements in ground-based Subaru observations ($\bar{n}_g \sim 30 - 40$arcmin^{-2}). However, we found that it is rather important to remove small/faint galaxy im-

ages and noisy outliers in flexion measurements since they are likely to be affected by the residual PSF anisotropy and/or observational noise in the shape measurement. Besides, the smaller the object, the larger the amplitude of intrinsic flexion contributions. Recall that flexion and HOLICs have a dimension of length inverse: The response to flexion is size-dependent, and the amplitude of intrinsic flexion is inversely proportional to the object size. Indeed, we find that inclusion of smaller objects results in a noisy reconstruction. Flexion measures essentially the gradient of the tidal gravitational shear field (i.e., $F, G \propto \phi(r)/r^3$), and hence is relatively sensitive to small-scale structures. Therefore, our successful reconstruction of the mass substructures with a small background density, $\bar{n}_g \sim 8\text{arcmin}^{-2}$, could be attributed to the superior sensitivity of flexion to small scale structures[8] and the here-adopted selection criteria for a background galaxy sample for weak lensing flexion analysis. Our flexion-based mass reconstruction of A1689 demonstrates the power of the generalized flexion analysis techniques for quantitative and accurate measurements of the weak gravitational lensing effects.

Acknowledgments

This work is partially supported by the National Science Council of Taiwan under the grant NSC95-2112-M-001-074-MY2.

References

1. M. Bartelmann and P. Schneider, *Phys. Rep.* **340**, 291 (2001).
2. K. Umetsu, M. Tada, and T. Futamase, *Prog. Theor. Phys. Suppl.* **133**, 53 (1999).
3. N. Kaiser, G. Squires, and T. Broadhurst, *ApJ* **449**, 460 (1995).
4. D. M. Goldberg and P. Natarajan, *ApJ* **564**, 65 (2002).
5. D. M. Goldberg and D. J. Bacon, *ApJ* **619**, 741 (2005).
6. D. J. Bacon *et al.*, *MNRAS* **365**, 414 (2006).
7. D. M. Goldberg and A. Leonard, *ApJ* **660**, 1003 (2006).
8. Y. Okura, K. Umetsu, and T. Futamase, *ApJ* **660**, 995 (2007).
9. Y. Okura, K. Umetsu, and T. Futamase, *ApJ*, in press (2007), arXiv:astro-ph/0710.2262.
10. T. Broadhurst *et al.*, *ApJ* **621**, 53 (2005).
11. T. Broadhurst, M. Takada, K. Umetsu *et al.*, *ApJ* **619**, L143 (2005).
12. M. Oguri, M. Takada, K. Umetsu, and T. Broadhurst, *ApJ* **632**, 841 (2005).
13. E. Medezinski, T. Broadhurst, and K. Umetsu *et al.*, *ApJ* **663**, 717 (2007).
14. K. Umetsu, M. Takada, and T. Broadhurst, *MPLA* **22**, 2099 (2007), astro-ph0702096.
15. K. Umetsu and T. Broadhurst, submitted to *ApJ* (2007), arXiv:astro-ph/0712.3441.
16. J. F. Navarro, C. S. Frenk, and S. D. M. White, *ApJ* **462**, 563 (1996).
17. A. Leonard *et al.*, *ApJ* **666**, L51 (2007).

This article has been cited by:

1. Björn Malte Schäfer, Lavinia Heisenberg, Angelos F. Kalovidouris, David J. Bacon. 2012. On the validity of the Born approximation for weak cosmic flexions. *Monthly Notices of the Royal Astronomical Society* **420**, 455-467. [CrossRef]